Progress in Oceanography 126 (2014) 109–120

Contents lists available at ScienceDirect

Progress in Oceanography

journal homepage: www.elsevier.com/locate/pocean

Direct breaking of large-amplitude internal waves in the Urup Strait

Sachihiko Itoh [a,*], Yuki Tanaka [b], Satoshi Osafune [c], Ichiro Yasuda [a], Masahiro Yagi [a], Hitoshi Kaneko [a], Shunsuke Konda [a], Jun Nishioka [d], Yuri. N. Volkov [e]

[a] Atmosphere and Ocean Research Institute, The University of Tokyo, Chiba, Japan
[b] Department of Earth and Planetary Science, The University of Tokyo, Tokyo, Japan
[c] Research Institute for Global Change, Japan Agency for Marine-Earth Science and Technology, Yokosuka, Japan
[d] Institute of Low Temperature Science, Hokkaido University, Sapporo, Japan
[e] Far Eastern Regional Hydrometeorological Research Institute, Vladivostok, Russia

ARTICLE INFO

Article history:
Available online 6 May 2014

ABSTRACT

Observations and model data have been analyzed for the Urup Strait, one of the Kuril Straits, focusing on processes driving the extremely strong vertical mixing. Observations over 1 day on the Pacific side of the sill of the Urup Strait show the generation of a large-amplitude internal wave (LAIW), characterized by the depression of potential density surfaces caused by a strong off-sill flow. When the LAIW developed, the potential density surface of 26.7 σ_θ was depressed downward by more than 300 m, and vertical mixing was markedly elevated within the 400-m-thick layer 26.6–26.7 σ_θ, with a layer-mean (maximum) energy dissipation rate and vertical diffusivity of 1.2×10^{-6} (7.9×10^{-6} W kg^{-1}) and 4.0×10^{-1} (2.8 m^2 s^{-1}), respectively. A three-dimensional model simulation of the Kuril Straits driven by the diurnal barotropic tide reproduces well the observed features relevant to the generation of LAIWs in and around the Urup Strait. The structure and generation pattern of LAIWs in the Urup Strait are consistent with those of the arrested lee waves observed in the Hawaiian ridge and Luzon Strait, although the depth at the top of the sill is far shallower in the Urup Strait. It is suggested that barotropic tidal energy with diurnal frequency is converted into LAIWs through the excitation of topographically trapped waves with hydraulically supercritical velocity near the sill top, and it is these waves that are responsible for the extremely strong mixing on the sill-flanks of the shallow Kuril Straits.

Introduction

The volcanic archipelago that forms the Kuril Islands separates the Sea of Okhotsk from the North Pacific (Fig. 1). The islands are themselves separated by passages or straits of varying scale, which are collectively called the Kuril Straits. The Kuril Straits are known for their strong diurnal tidal flows (Katsumata et al., 2001; Rabinovich and Thomson, 2001; Ohshima et al., 2002; Katsumata et al., 2004), and vertical mixing driven by the tidal flow is thought to contribute to the formation and modification of intermediate water in the Sea of Okhotsk and the North Pacific (Kitani, 1973; Talley, 1991; Yasuda, 1997). Mixing in and around the straits is also thought to play an important role in bidecadal variability in temperature, salinity, nutrient concentrations, and dissolved oxygen concentration, possibly through the modification of tidal amplitude by the 18.6-year nodal tidal cycle (Osafune and Yasuda, 2006; Watanabe et al., 2008; Tadokoro et al., 2009).

The Urup Strait is a shallow passage between the Urup and Chirpoy Islands, southwest of the deepest passage, the Bussol' Strait (Fig. 1b). The width of the Urup Strait, measured as the distance between the Urup and Chirpoy islands, is about 30 km, and the main channel is located on a steep sill with depth of about 100 m. Because the horizontal and vertical scales of the Urup Strait are smaller than those of major straits such as the Bussol' and Krusenstern straits (which are 80–100 km width, with maximum depth exceeding 1500 m), its role in water exchange between the Pacific and Okhotsk may be minor (Nakamura et al., 2000a). However, in contrast to the small volume transport, tidal velocities in the shallow straits tend to be stronger than in the deep straits. In numerical models, interaction between the strong tidal flow and steep topography drives extremely strong mixing (Nakamura et al., 2000b; Nakamura and Awaji, 2004; Tanaka et al., 2007, 2010). Numerical experiments indicate that the depth-integrated energy dissipation rate exceeds 1 W m^{-2} at the sill-break of the Urup Strait (Tanaka et al., 2007, 2010). Integrated energy dissipation rates exceeding 1 W m^{-2} have also been estimated in other

* Corresponding author. Address: Center for Earth System Dynamics, Atmosphere and Ocean Research Institute, The University of Tokyo, 5-1-5 Kashiwanoha, Kashiwa, Chiba 277-8564, Japan. Tel.: +81 4 7136 6326; fax: +81 4 7136 6327.
E-mail address: itohsach@aori.u-tokyo.ac.jp (S. Itoh).

http://dx.doi.org/10.1016/j.pocean.2014.04.014
0079-6611/

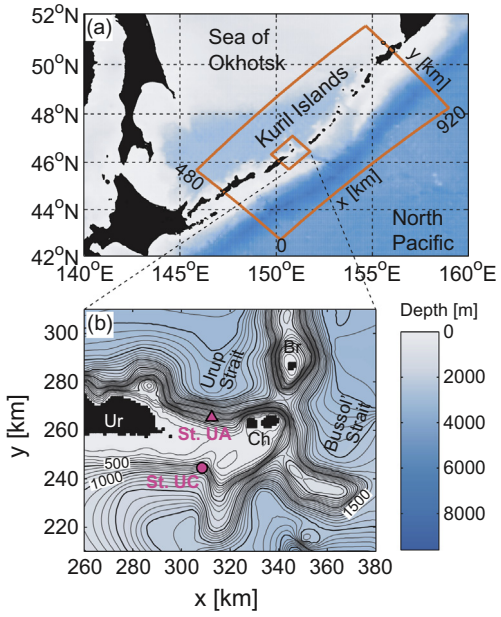

Fig. 1. Study site, showing (a) the Kuril Straits and (b) the focused area including the Urup Strait and the southwestern part of the Bussol' Strait. The large orange box indicates the domain of the numerical experiments. In (b), observation stations UA (conducted in 2006, and denoted "St. A" in Itoh et al., 2011) and UC (conducted in 2007 and revisited in the present study, denoted "St. C" in Itoh et al., 2011) are shown by a pink triangle and circle, respectively. Urup Island, the Chirpoy Islands, and Broutona Island are labeled Ur, Ch, and Br, respectively. (For interpretation of the references to color in this figure legend, the reader is referred to the web version of this article.)

shallow straits, especially around the sill-break; these are higher than those in the deep channels in the eastern part of the Bussol' and Krusenstern straits (fig. 5 of Tanaka et al., 2010).

The first direct estimation of the vertical mixing (turbulent kinetic energy dissipation rate, ε) in the Kuril Straits was conducted in August 2006 using microstructure profilers. In the Urup Strait, profiles of temperature, salinity, velocity, and microstructure were repeatedly taken at the Okhotsk-side of the sill over 1 day during neap tide (Itoh et al., 2010). Intense turbulence was observed, associated with a large depression of isopycnal surfaces during the off-sill flow, or with strong vertical shear of horizontal velocity. While the former process was interpreted as the direct breaking of a large-amplitude internal wave, the latter was attributed to interactions between propagating internal waves and background shear. However, the mean ε over the day of about 2×10^{-8} W kg^{-1} (corresponding to a vertical diffusivity K_ρ of $\sim 10^{-3}$ m^{-2} s^{-1}), yielding vertically integrated energy dissipation rates of $\sim$0.02 W m^{-2}, was smaller than the 1 W m^{-2} estimated by the models.

Microstructure observations were also performed in August 2007 at three stations on the Pacific side of the sill during spring tide. Extremely strong mixing was observed on the flank of the sill, with ε of 10^{-6} to 10^{-5} W kg^{-1} and K_ρ of 10^{-1} to 5×10^{-1} m^{-2} s^{-1}. The 1-day mean ε of 10^{-6} W kg^{-1} corresponds to a vertically integrated energy dissipation rate of $\sim$1 W m^{-2}, comparable with model estimates (Tanaka et al., 2007, 2010). The enhanced mixing occurred during periods of off-sill flow or during the transition periods from off-sill to on-sill flow that accompanied the depression of isopycnal surfaces, consistent with the observations in 2006. However, because these two sets of observations were conducted at different sites during different parts of the lunar cycle (i.e., one on the Okhotsk side during neap tide and the other on the Pacific side during the spring tide), more data were needed to confirm the mixing intensity and the processes enhancing turbulence.

While tidal energy cascades down through various processes (e.g., Garrett and Kunze, 2007), the importance of direct breaking of large-amplitude internal waves has recently been highlighted at several locations with prominent topography such as the Hawaiian ridge (Klymak et al., 2008; Legg and Klymak, 2008), the Amchitka Pass in the Aleutian Islands (Nakamura et al., 2010), and the Luzon Strait (Klymak et al., 2012; Pinkel et al., 2012). Klymak et al. (2010b) parameterized the energy dissipation caused by the direct breaking of internal waves on the assumption that internal waves with slower phase speed than the tidal advection speed are arrested and dissipate locally; this explains the energy dissipation over the Kauai ridge of Hawaii calculated in numerical experiments.

Although the term "lee wave" has often been assigned strictly to the stationary wave generated on the lee side of the slope under non-hydrostatic conditions that allow internal wave energy to propagate downstream, the arrested wave on the lee side of a steep topography examined by Klymak et al. (2010b) was also termed a lee wave. As investigated by Klymak et al. (2010a), a highly nonlinear wave referred to as an "arrested lee wave" is generated on the lee-side of a steep and tall obstacle. When the topography is high enough so that the topographic Froude number $Nh_m/U_o \gg 1$ (where N, h_m, and U_o are buoyancy frequency, height of the topography, and undisturbed barotropic velocity, respectively), the lower part of the water is blocked. In this case the horizontal wavenumber k is scaled by the effective width of the topography where vigorous tide–topography interaction occurs, and the horizontal velocity U is scaled by that at the top of the topography, U_m, instead of U_o. Assuming that the ratio of horizontal and vertical wavenumbers k/m was scaled with the effective aspect ratio of the topography α, Klymak et al. (2010a) derived the intrinsic frequency of the arrested lee wave as $\omega = Nk/m \sim \alpha N$ using the hydrostatic approximation. In the present study, this wave examined by Klymak et al. (2010a,b) is termed the arrested lee wave. However, as both the diurnal and semidiurnal tides are superinertial in the Hawaiian ridge, it is yet to be confirmed whether the arrested lee wave is generated similarly in areas of subinertial tide, such as the Kuril Straits and the Aleutian Straits.

A numerical simulation for the Kuril Strait area driven by the subinertial diurnal tide suggested the breaking of waves with small spatial scale generated at the sill-breaks. Nakamura et al. (2000b) therefore attributed the strong mixing in the Kuril Straits to these waves, which they termed "unsteady lee waves", defined as a variant of a steady lee wave. These waves were assumed to be excited by a strong oscillatory flow of $U_0 \gg \sigma_f/k$, and have an intrinsic frequency $-kU_0 \pm \sigma_f$, where k, U_0, and σ_f are a horizontal wavenumber, barotropic tidal amplitude, and tidal frequency, respectively. Although the theoretical background of the unsteady lee waves is still under discussion (e.g., Tanaka et al., 2010), the results of two-dimensional (Nakamura et al., 2000b) and three-dimensional (Nakamura and Awaji, 2004) numerical experiments clearly show that isopycnal surfaces are depressed at the lee-side of the topography, resulting in wave breaking and the radiation of wave-like disturbances.

Tanaka et al. (2010) also performed three-dimensional numerical experiments for the Kuril Straits, but paid more attention than Nakamura and Awaji (2004) to the diurnal internal tides that are dominant around the ridge. Because the diurnal tide is subinertial in the Kuril Straits, the diurnal baroclinic tides do not propagate freely, but are trapped along the topography as shelf waves, referred to as topographically trapped waves (TTWs, equivalent to the term "coastal trapped waves" of Tanaka et al., 2010). Tanaka et al. (2010) showed that the internal tide was mostly trapped near the topography as TTWs, and more than 80% of the tidal energy was dissipated locally near the ridge. The vertical shear of horizontal velocity became strong near the bottom as

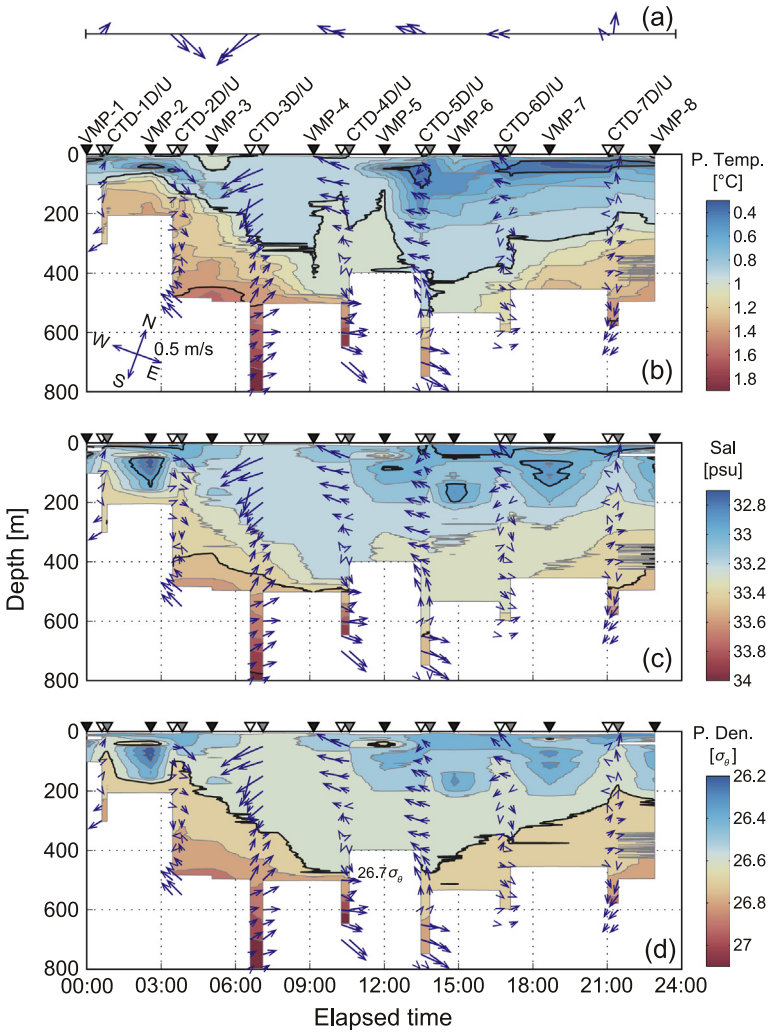

Fig. 2. Observations over 1 day of (a) mean horizontal velocity above 26.7 σ_θ, (b) potential temperature, (c) salinity, and (d) potential density overlain with horizontal velocity observed at St. UC in the Urup Strait. All variables are plotted against the time since the first VMP deployment. Gray (black) contours are drawn at intervals of (b) 1 °C (5 °C) and (c) 0.1 psu (0.5 psu). In (d), gray lines are contours with interval 0.1 σ_θ, while black lines indicate the 26.7 σ_θ isopycnal. Velocity vectors are rotated so that toward the top of the panel indicates the on-sill (340°) orientation. Black, white, and gray triangles at the top of each panel denote the start time of the VMP, descending CTD, and ascending CTD measurements, respectively.

TTWs were enhanced, and Tanaka et al. (2010) assumed that this shear drove bottom-confined strong mixing. However, the detailed processes of TTW dissipation were not explained. The large-amplitude disturbance found on the lee-side of the sill in their model (their Fig. 7) suggests that energy dissipation from TTWs occurs through the generation of large-amplitude internal waves, especially at shallow straits such as the Urup Strait.

In the present paper, to elucidate the processes causing extremely strong vertical mixing in the Kuril Straits, we analyze data from direct observations conducted in 2010 in the Urup Strait during neap tide, and the results of three-dimensional numerical experiments performed by Tanaka et al. (2010). The remainder of this manuscript is organized as follows. Details of the observations and the model data analysis are given in 'Data and analysis methods'. In 'Observations in the Urup Strait, May 2010', we assess the temporal and vertical variations in flow, water mass, and energy dissipation rates in the Urup Strait based on the observations over 1 day at the Pacific side of the sill. The model results are first compared with observations at sites in the Urup Strait, and 'Model data analysis' presents the three-dimensional variations in horizontal velocity, potential density, and energy dissipation rates around the Urup Strait. Finally, the mixing intensity in the Urup Strait, the impacts of breaking of large-amplitude internal waves, and the role of shallow straits such as the Urup Strait in water mass formation are discussed in 'Discussion and conclusions'.

Data and analysis methods

Observations

Observations over 1 day were conducted at Station UC (Station C of Itoh et al., 2011) on the Pacific side of the Urup Strait during neap tide, in May 2010. Over the course of the day, a vertical microstructure profiler (VMP: VMP500, Rockland Scientific International) and a conductivity–temperature–depth profiler (CTD: SBE911plus, Sea-Bird Electronics) mounted on the same frame as a lowered acoustic Doppler current profiler (LADCP: Workhorse 300 kHz, Teledyne RD Instruments) were alternately deployed 8 and 7 times, respectively. For the CTD and LADCP, profiles taken during both descending and ascending casts were used. The VMP and CTD casts are numbered sequentially, as VMP-1, VMP2, and CTD-1D, CTD-1U, CTD-2D, CTD-2U, where "D" and "U" denote descending (downward) and ascending (upward) casts, respectively.

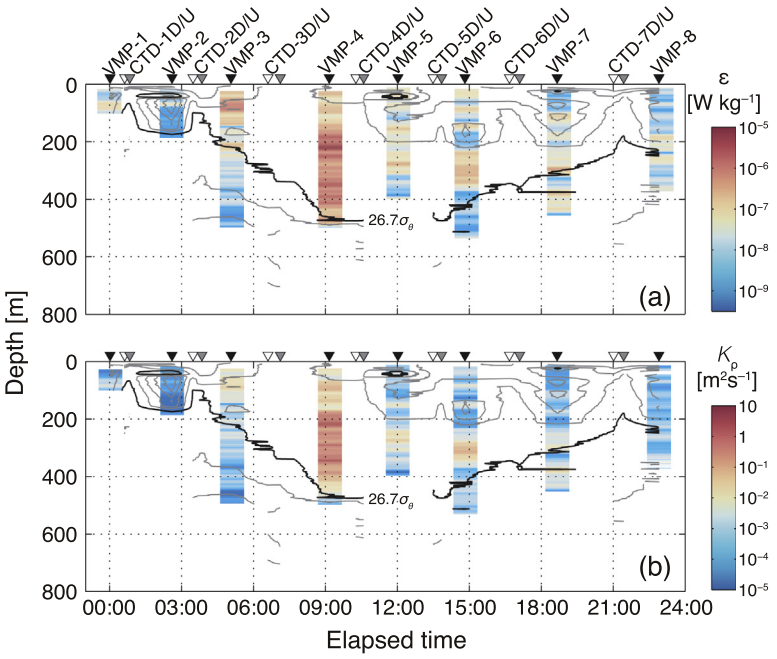

Fig. 3. As for Fig. 2 but for (a) turbulent energy dissipation rate and (b) vertical diffusivity. Potential density contours are overlain as gray and black lines, and timings are shown by triangles at the top of the panels, as for Fig. 2.

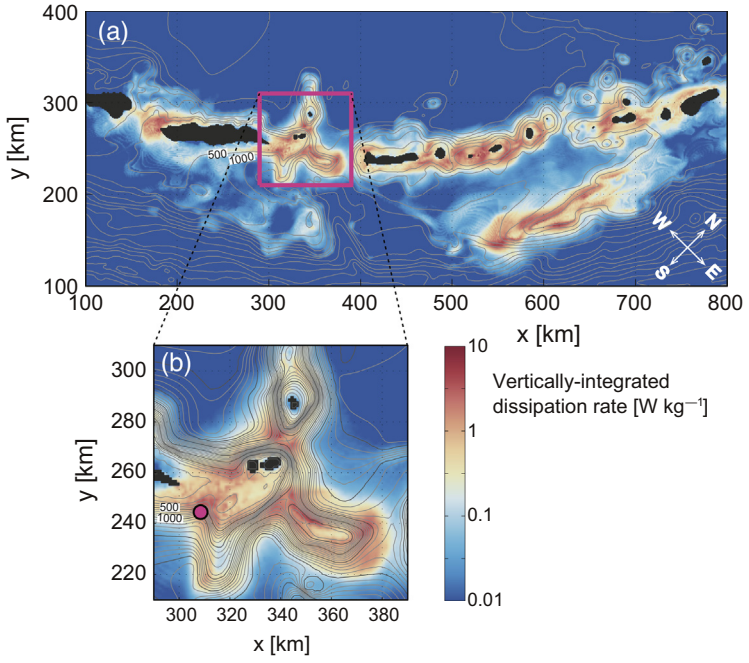

Fig. 4. Depth-integrated energy dissipation rates (a) of the Kuril Straits and (b) around the Urup Strait. Gray contours indicate bottom topography with contour intervals of 500 m. A pink circle within the Urup Strait indicates the location of Station UC.

Turbulent energy dissipation rates ε were estimated from micro-scale velocity data measured by the VMP. We employed the same data processing method as Itoh et al. (2010). Vertical diffusivity was calculated from ε as $K_\rho = \Gamma\varepsilon/N^2$ (Osborn, 1980), where we assume $\Gamma = 0.2$.

Raw LADCP data were processed using LDEO software (Thurnherr, 2011), based on an inverse technique developed by Visbeck (2002). Because the LADCP data at CTD-2U could not be processed properly due to the rapid drifting of the ship across the steep topography, the horizontal velocity profile at CTD-2U is not presented. Although the bottom topography employed by Tanaka et al. (2010) implies an on-sill direction of ~315° (Fig. 1), we present the observed velocity data with the vectors rotated 20° anticlockwise (such that the orientation of 340° is at the top of the figures) to be consistent with Itoh et al. (2011), because the detailed topography near Station UC has not been confirmed.

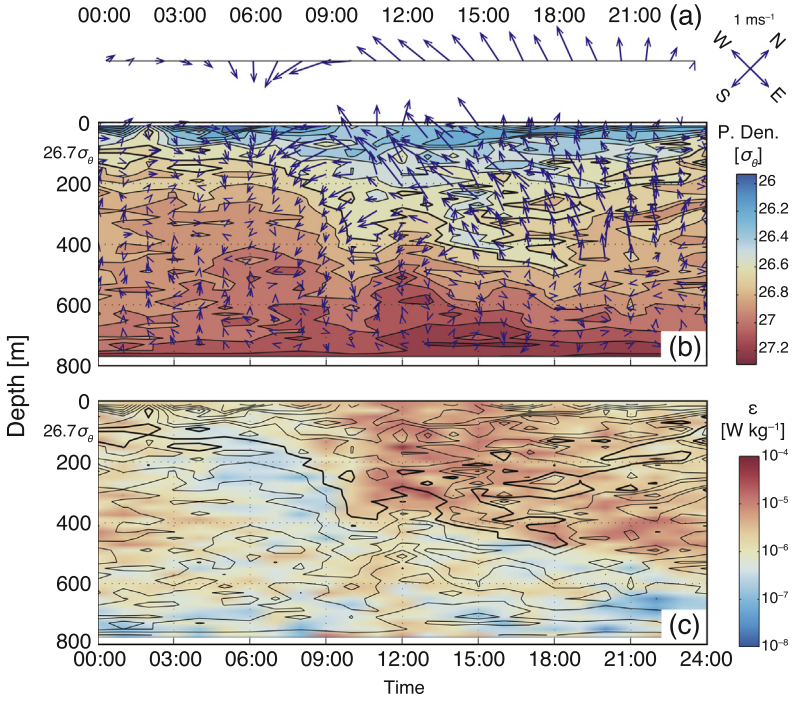

Fig. 5. Time variations in horizontal velocity, potential density, and energy dissipation rates calculated by the model for the observation sites in the Urup Strait (Station UC) over the 10th model day: (a) mean velocity above 26.7 σ_θ, (b) potential density (filled contour) and horizontal velocity (vectors), and (c) energy dissipation rate (color shading) and potential density (black contours). Thin contours of potential density are drawn with an interval of 0.1 σ_θ, while the thick contours indicate the 26.7 σ_θ isopycnal. (For interpretation of the references to colour in this figure legend, the reader is referred to the web version of this article.)

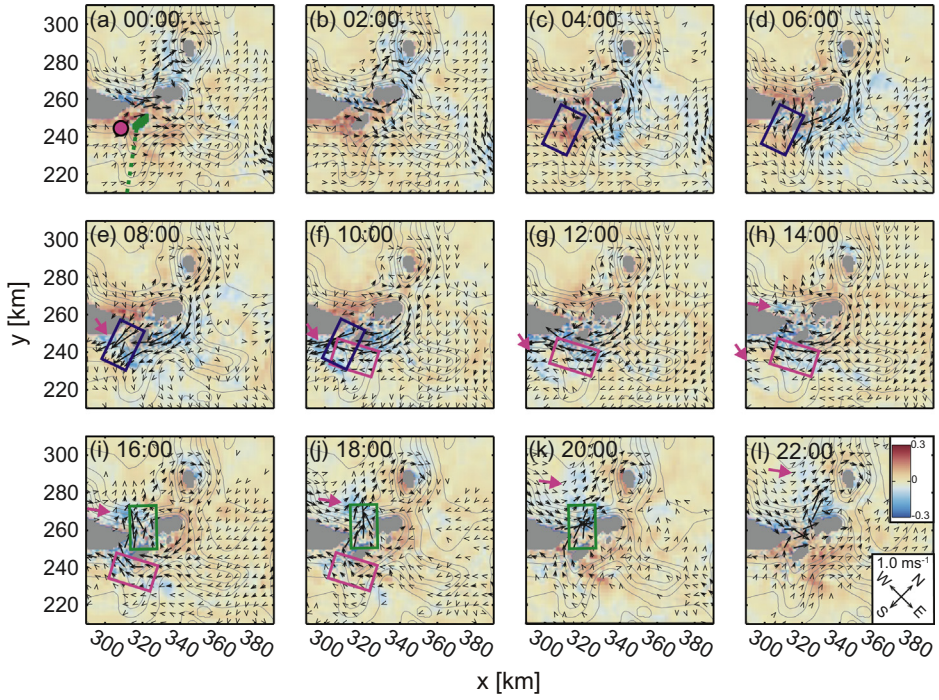

Fig. 6. Time series of potential density anomalies [σ_θ] from the 24-h mean at 90 m (color shading) and of horizontal velocity at 90 m (vectors) around the Urup Strait for model times from 0:00 to 22:00. Velocity vectors are drawn at 5-km intervals, and those slower than 0.01 m s^{-1} are not shown. Thin gray lines indicate contours of bottom depth with a 500 m interval, and gray areas are those shallower than 90 m. In (a) the rise within the Urup Strait is colored green, and the small ridge extending from the rise is indicated by a pink dashed line. Blue, pink, and green boxes indicate areas and periods of off-sill flows. Pink arrows indicate the propagating disturbances. (For interpretation of the references to color in this figure legend, the reader is referred to the web version of this article.)

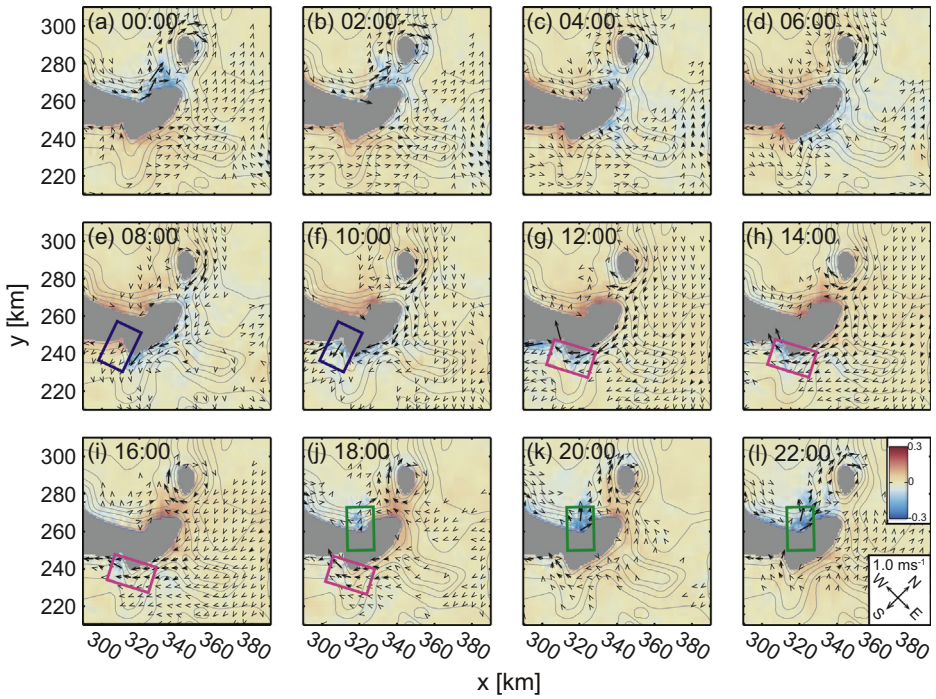

Fig. 7. As for Fig. 6 but for potential density anomalies from the 24-h mean at 290 m (color shading) and for horizontal velocity at 290 m (vectors). (For interpretation of the references to color in this figure legend, the reader is referred to the web version of this article.)

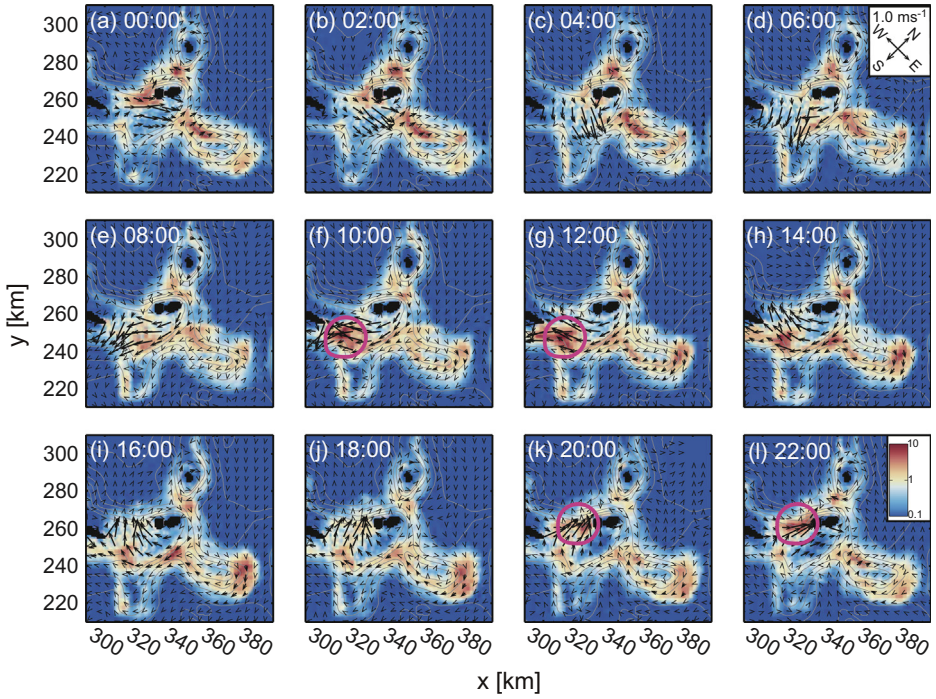

Fig. 8. As for Fig. 6 but for depth-integrated energy dissipation rates (color shading) and for depth-averaged horizontal velocity (vectors). Pink circles indicate peaks in the depth-integrated energy dissipation rates. (For interpretation of the references to color in this figure legend, the reader is referred to the web version of this article.)

Model data

The model data used in the present study were derived from the numerical experiment by Tanaka et al. (2010), which used a three-dimensional model for the Kuril Straits driven by the K_1 barotropic tide (Fig. 1). The model was run with a horizontal grid spacing of 1000 m, and a vertical grid spacing of 20 m in the upper 1800 m. Horizontal and vertical viscosity and diffusivity coefficients were assumed to be constant, with values of horizontal viscosity and diffusivity of 10 and 10^{-3} m^2 s^{-1}, and vertical viscosity and diffusivity of 1 and 10^{-4} m^2 s^{-1}, respectively. Changing these parameters by a factor of 5 resulted in only minor differences in the energy budget (Tanaka et al., 2010). A second-order central-difference advection scheme was employed. We analyze the model outputs for surface

elevation, horizontal velocity, potential density (a constant value of 4.72 kg m^{-3} is subtracted from the original record with a reference pressure of 1000 dbar to derive the potential density referenced at 0 dbar), and energy dissipation rates (sum of horizontal and vertical viscous energy losses), recorded for the 10th model day at hourly intervals. As in Tanaka et al. (2010), the coordinates x and y are oriented toward the northeast and northwest, respectively. Further specifications of the parameters and settings of the model may be found in Tanaka et al. (2010).

Results

Observations in the Urup Strait, May 2010

Potential temperature, salinity, and potential density profiles showed large variations over the day (Fig. 2). An isosurface of potential density 26.7 σ_θ, approximately corresponding to 1.1 °C and 33.3 psu, was observed at depths shallower than 200 m until 4:00 (CTD-2U); it reached depths greater than 450 m at 10:30 (CTD-4U), and was again observed around 200 m depth at 23:00. The depression of the 26.7 σ_θ surface was followed by homogenization of the upper layer, typically during 6:30–10:30 (CTD-3D to CTD-4U). This layer was more than 300 m thick, with potential temperature of 0.9–1.1 °C, salinity of 33.2–33.3 psu, and potential density of 26.6–26.7 σ_θ. Once the maximum depression of the 26.7 σ_θ surface was reached, the upper layer began to be covered by colder and fresher water to become stratified again.

The downward depression of the 26.7 σ_θ isopycnal observed during 3:30–7:00 (from CTD-2D to CTD-3U) occurred with an off-sill flow of 0.15–0.27 m s^{-1} averaged above 26.7 σ_θ, with maximum at CTD-3D. The mean cross-sill flow above 26.7 σ_θ was on-sill (toward Okhotsk) in the other casts, except for CTD-6D where it was slightly off-sill, with magnitude less than 0.01 m s^{-1}. The mean along-sill component above 26.7 σ_θ mostly flowed with the sill top on its right. The velocity vectors rotated clockwise with time. Although the profile depths varied as the ship drifted during and between CTD deployments in areas with extremely steep slope, available data below 26.7 σ_θ suggest that the direction of flow was opposite to that of the upper layer, especially from 3:30 to 15:00 (from CTD-2D to CTD-5U). Note that these general results do not change even under the assumption that the on-sill direction is 315° (rotating the vectors in Fig. 2 clockwise by 25°), as suggested by the topography employed in the model.

Although the observations were conducted during neap tide, mixing intensity was remarkably high (Fig. 3). Strong mixing was observed when the 26.7 σ_θ isopycnal was at its greatest depth at 9:00 (VMP-4), within the homogenized layer of 26.6–26.7 σ_θ from 50 to 450 m. Strong vertical mixing concentrated in this layer has been linked to the formation of intermediate waters in the Sea of Okhotsk and the North Pacific (Itoh et al., 2011). Intensities of the mixing inside and outside of the 26.6–26.7 σ_θ layer are compared in detail here. Mean and maximum of ε and K_ρ within the 26.6–26.7 σ_θ layer at VMP-4 were 1.2×10^{-6} W kg^{-1} and 4.0×10^{-1} m^2 s^{-1}, and 7.9×10^{-6} W kg^{-1} and 2.8 m^2 s^{-1}, respectively. Although ε and K_ρ observed in casts other than VMP-4 were mostly below 1×10^{-6} W kg^{-1} and 1×10^{-2} m^2 s^{-1}, respectively, elevated values were observed in the 26.6–26.7 σ_θ layer of each cast. Mean ε within the 26.6–26.7 σ_θ layer calculated from all available data was 5.3×10^{-7} W kg^{-1}, ten times higher than the 4.8×10^{-8} W kg^{-1} calculated from the data above and below this layer.

The overall results of the observations in the Urup Strait conducted in 2010 are basically consistent with those in 2006 and 2007 (Itoh et al., 2010, 2011): downward depression of isopycnal surfaces occurred with the off-sill flow, followed by strong mixing. As mentioned in previous studies, we regard this as a breaking of large-amplitude internal waves. Moreover, these variations in isopycnal surfaces and enhanced mixing were observed in the similar potential density range of 26.6–26.7 σ_θ for both 2007 and 2010, despite the difference in season (August and May, respectively) and lunar phase (spring and neap, respectively). Detailed comparisons and a discussion of the mechanism enhancing the strong mixing are given in 'Discussion and conclusions'.

Model data analysis

This section analyses the output of the numerical experiment performed by Tanaka et al. (2010). First, the horizontal distribution of water-column integrated energy dissipation rates is reviewed to characterize the Urup Strait relative to the various Kuril Straits. Then, a direct comparison is made between the observations and model output over a 24-h period at the same location. Fluctuations in the spatial structure are considered next, focusing on the depression of isopycnals on the lee-side of the sill, which we regard as representing the large-amplitude internal waves in the observations. The structure and propagation across the ridge are also analyzed, to understand the properties of the waves.

Variation around the Urup Strait

A three-dimensional numerical experiment by Tanaka et al. (2010) reproduced large energy dissipation confined around the Kuril Straits (their Fig. 5), consistent with estimates using altimetry data and a barotropic tidal model (Tanaka et al., 2007). Fig. 4a is similar to Fig. 5 of Tanaka et al. (2010) (although it focuses on the region defined by 100 km $\leqslant x \leqslant$ 800 km and 100 km $\leqslant y \leqslant$ 400 km), and the finer depth resolution of the contours reveals that the largest energy dissipation occurs around the edge of prominent topography, such as sill-breaks. These hot spots, with mean depth-integrated energy dissipation rates typically greater than 1 W m^{-2}, occupy 0.5% of the water volume in the model domain (excluding the 50 km-wide edge along each open boundary), but account for 48% of the total energy dissipation.

Within the Urup Strait, there are hot spots of depth-integrated energy dissipation rates around both the northwestern and southeastern sides of the sill, where the bottom depth ranges from about 100 to 1000 m (Fig. 4b). The areas slightly below the sill-breaks are hereafter referred to as sill-flanks. High energy dissipation rates are also estimated on sill-flanks of the western ridge within the Bussol' Strait and sill-flanks of the passage between the Chirpoy and Broutona Islands. It is noted that Station UC is located almost at the center of the hot spot.

Even though the model was driven simply by the K_1 component of the barotropic tide, starting from a horizontally uniform initial condition, it reproduces well the characteristics of the flow and potential density structure at Station UC on the Pacific side of the sill-flank (Fig. 5). Isopycnals were rapidly depressed downward with an off-sill flow emerging for a limited period from approximately 5:00 to 10:00. The amplitude of the displacement exceeds 200 m, with the 26.7 σ_θ isopycnal reaching 400 m depth. As in the observations, this rapid depression is followed by high energy dissipation rates exceeding 10^{-5} W kg^{-1} within the layer above 26.7 σ_θ. While Tanaka et al. (2010) have already validated the general performance of the model, these results further indicate that the model correctly reproduces the processes causing extremely strong mixing in the Urup Strait.

To clarify the processes causing the downward depression, temporal variations in the horizontal fields of velocity, potential density, and energy dissipation rates are examined (Figs. 6–8). Although the 26.7 σ_θ isopycnal is depressed down to 400 m depth (Fig. 5), the depth of the main passage of the Urup Strait on the sill top is 130 m at most. We therefore examine time series of horizontal velocity and potential density at 90 m and 290 m depths. The

former shows the variability within the whole Urup Strait, while the latter corresponds to the level where the variations in the isopycnals are prominent (Fig. 5). At the 90 m depth level in the model, the Urup Strait is divided into two by a rise shallower than 90 m (Fig. 6a; x = 320 km, y = 250 km, hereafter referred to as "the rise"): the main western channel directly connects the North Pacific to the Sea of Okhotsk, while the northern channel connects the Sea of Okhotsk to the southwestern part of the Bussol' Strait. There is, however, no passage between the Pacific and the Okhotsk in the Urup Strait at 290 m depth (Fig. 7).

The flow around the Urup Strait does not simply pass through the middle of the Urup Strait but rotates horizontally and interacts with the flow from the Bussol' Strait. Because a small ridge (Fig. 6a; x = 320 km) extends southeast from the rise, the flow at Station UC (Fig. 6a; x = 309 km, y = 244 km) is aligned off-sill not only when it passes through the main passage of the Urup Strait (4:00–10:00 at 90 m, blue boxes in Fig. 6c–f; 8:00–10:00 at 290 m, blue boxes in 7e–f), but also when it comes through the western end of the Bussol' Strait (10:00–18:00 at 90 m, pink boxes in Fig. 6f–j; 12:00–18:00 at 290 m, pink boxes in Fig. 7g–j). On the Okhotsk flank of the sill, the off-sill flow is excited simply by the cross-sill flow in the main passage, which is evident from 16:00 to 20:00 at 90 m (green boxes in Fig. 6i–k) and from 18:00 to 22:00 at 290 m (green boxes in Fig. 7j–l).

Off-sill flows on the sill-flanks are generally followed by prominent negative (light) anomalies of potential density, indicating the depression of isopycnal surfaces (Fig. 5), both on the Pacific (6:00–18:00 at 90 m, Fig. 6d–j; 10:00–18:00 at 290 m, Fig. 7f–j) and the Okhotsk sides (16:00–20:00 at 90 m, Fig. 6i–k; 18:00–22:00 at 290 m, Fig. 7j–l). Disturbances emanating from these negative potential density anomalies are detected to the south from the Pacific side of the ridge from 8:00 to 14:00 at 90 m (pink arrows in Fig. 6e–h), and to the northwest from the Okhotsk side of the ridge from 16:00 to 20:00 at 90 m (pink arrows in Fig. 6i–k).

Variations of the depth-integrated energy dissipation rates on the two sill-flanks of the Urup are out of phase (Fig. 8). The peak energy dissipation rates as indicated by pink circles in Fig. 8 occur from 10:00 to 12:00 (Fig. 8f–g) for the Pacific side, and from 20:00 to 22:00 (Fig. 8k–l) for the Okhotsk side. The timings of these peaks correspond approximately to the deep isopycnal depressions caused by the off-sill flows seen at 290 m (Fig. 7).

Variability across the ridge

The large-amplitude depressions of the isopycnal surfaces in the Urup Strait associated with the off-sill flows are not attributable to fluctuations of the low-mode TTWs propagating along isobaths (Tanaka et al., 2010). As the structure and fluctuation of the depressions are consistent with observations from the present and previous studies (Itoh et al., 2010, 2011), we follow Itoh et al. (2010, 2011) in referring to these disturbances as large-amplitude internal waves (LAIWs). Although the fluctuations within the Urup Strait are more complex than simple two-dimensional oscillatory flow, we detect the propagation of disturbances toward the northwest and the south of the Urup Strait (Fig. 6). Therefore, we analyze the spatio-temporal variability along lines located northeast and south of the ridge of the Urup Strait.

The normalized surface elevation anomalies are seen to propagate away from the Urup Strait toward the North Pacific and the Sea of Okhotsk, along the lines P and O, respectively, as shown in Fig. 9. The marked positive disturbances emanating from the Pacific sill-flank (r = −18 km: Fig. 9c) at 8:00 and the Okhotsk-side sill-flank (r = 10 km: Fig. 9b) at 14:00 propagate with approximate speeds of 0.78–1.3 and 0.56–1.3 m s^{-1}, respectively; they correspond approximately to the negative potential density anomalies at 90 m. In front of the fastest propagating positive elevation anomalies, velocity vectors are broadly aligned away from the ridge along P and O (downward in Fig. 9c and upward in Fig. 9b), which is consistent with the structure of propagating inertia-gravity waves (Gill, 1982). Velocity vectors of other propagating disturbances, including those with slower propagation speed behind the front, are not aligned with P or O, suggesting propagation in other directions.

Fig. 10 shows cross-sections of potential density anomalies and velocity components along the lines P and O for the periods of LAIW generation and for the propagating waves detected in Fig. 9. The off-sill flows extend down from the sill from 08:00 to 10:00 on the Pacific side (from 16:00 to 18:00 on the Okhotsk side), enhancing the negative potential density anomalies that denote the LAIWs (see Figs. 5–8), and a complex interleaving structure develops by 12:00 on the Pacific side (at 20:00 on the Okhotsk side). The progressive wave fronts detected in Fig. 6 and Fig. 9 emanate from intense cross-slope velocity components corresponding to LAIWs.

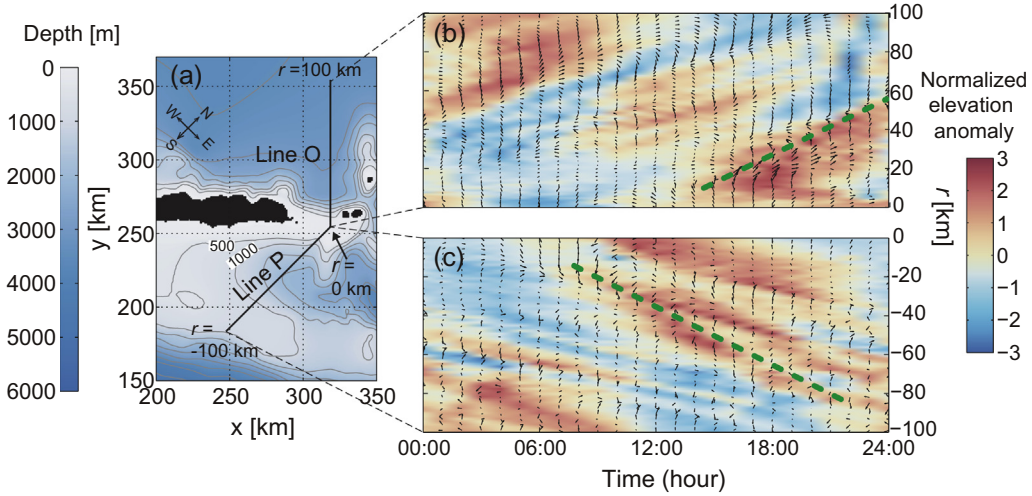

Fig. 9. Hovmöller diagrams of the normalized surface elevation anomalies (color shading) and the normalized horizontal velocity at 10 m (vectors) along transects away from the Urup Strait. (a) Location of the lines toward the Pacific (Line P) and the Okhotsk (Line O), (b) and (c) Hovmöller diagrams along Lines O and P, respectively. To eliminate barotropic tide signals with large spatial scale, along-line means from 30 to 100 km and −30 to −100 km are first subtracted from the raw records of surface elevation and horizontal velocity, and then the data are normalized with respect to time. (For interpretation of the references to color in this figure legend, the reader is referred to the web version of this article.)

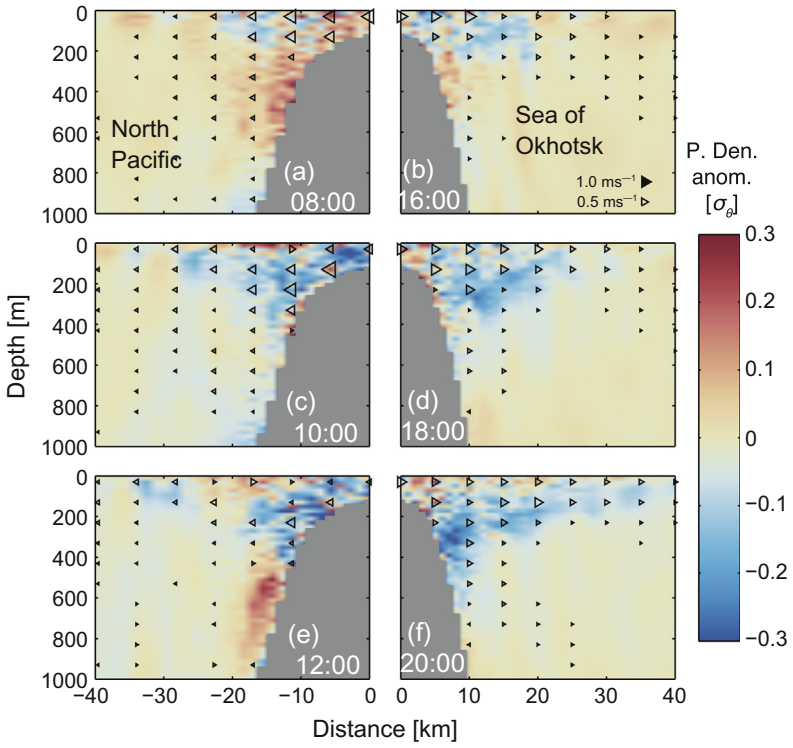

Fig. 10. Cross-sections of potential density anomalies from the 24-h mean values (color shading) and horizontal velocity (plotted with horizontal and vertical intervals of 5 km and 100 m, respectively) along lines P (a, c, and e) and O (b, d, and f). Leftward (rightward) pointing triangles indicate the velocity away from the ridge, and the area of the triangles represents the magnitude of the velocity. Velocity vectors with magnitude greater than 1 m s^{-1} are shown as black triangles, while those with magnitude less than 5 cm s^{-1} are not plotted. (For interpretation of the references to color in this figure legend, the reader is referred to the web version of this article.)

Although the model is driven by the diurnal tide, the LAIWs last for only a fraction of the diurnal tidal cycle near the ridge. As seen in Fig. 10, the enhanced off-sill flows generate the LAIWs with an aspect ratio similar to the top of the sill. The linear hydrostatic dispersion relation $\omega^2 = k^2N^2/m^2 + f^2$ (k, m, and f are the horizontal wave number, the vertical wave number, and the inertial frequency, respectively) indicates that the generated LAIWs have an intrinsic frequency ω independent of the tidal frequency. Their aspect ratio is estimated as $\alpha = 0.05$, based on the horizontal and vertical extents of negative potential density anomalies at the sill-flank (~10 km and ~500 m, respectively; Fig. 10c–f), Their intrinsic frequency, αN, is estimated roughly as 2.2×10^{-4} s^{-1} (corresponding to a period of 7.8 h) using the mean buoyancy frequency of 4×10^{-3} s^{-1} in the upper layer. Although these estimations by eye are approximate, the horizontal scale of the negative potential density anomaly (half the wavelength) is obviously not determined by the full width of the sill (20–25 km, as measured from the top to the base where the bottom depth is ~3000 m), but is related to the "effective width" (Klymak et al., 2010a) of the sill that is likely relevant to the vertical scale of the negative potential density anomaly.

Propagating away from the sill, the negative potential density anomalies decrease in amplitude and their spatial extent is modified (Fig. 10e–f). The propagation speed of 1.3 m s^{-1} and horizontal wavelength of ~ 30 km recognized in Fig. 9 require a vertical wavelength of $\geqslant$1500 m (~1700 m, assuming $N = 4 \times 10^{-3}$ s^{-1}), suggesting a modification to the low vertical mode structure.

Discussion and conclusions

Large-amplitude internal waves

Results of the 1-day observations and the three-dimensional numerical simulations have both shown strong mixing on the lee-side of the sill of the Urup Strait, following the generation of a large-amplitude internal wave (LAIW) caused by the off-sill flow. The vertical scale and generation pattern of the LAIWs are consistent with previous observations in the Urup Strait (Itoh et al., 2010, 2011). While neither the observations nor the model can resolve the cascading processes from the LAIWs to viscous dissipation, it is reasonable to conclude that the strong mixing is caused by breaking of LAIWs.

The structure and generation pattern of LAIWs are similar to those of unsteady lee waves (Nakamura et al., 2000b; Nakamura and Awaji, 2004) and arrested lee waves (Legg and Klymak, 2008; Klymak et al., 2010a,b). All these waves are amplified on the lee-side of steep topography, characterized by the depression of isopycnal surfaces; in addition, they break directly, giving high energy dissipation rates. The generation of these waves is obviously different from the linear response to tidal flow, such as freely propagating internal waves generated by a superinertial tide or TTWs by subinertial tide. As in Klymak et al. (2010b), the development of arrested lee waves over high topography requires that the intrinsic frequency αN is greater than the tidal frequency, because the waves need time to be established before the flow reverses.

According to Nakamura et al. (2000b), unsteady lee waves are generated when the tidal amplitude is large enough so that $U_0 \gg \sigma_f/k$. Although the theoretical validity of the intrinsic frequency $-kU_0 \pm \sigma_f$ is still under discussion (Tanaka et al., 2010), this condition is actually equivalent to that for the arrested lee wave over high topography, because kU_0 is the maximum frequency of the quasi-steady lee wave generated by oscillatory flow (Mohri et al., 2010). In the case of high topography, as for the Kuril Straits where $Nh_m/U_o \gg 1$, the horizontal wavenumber k is determined by the effective width of the topography that depends on the vertical wave number m, as shown by Klymak et al. (2010a), rather than simply by the full width. Although Nakamura et al. (2000b) did not explicitly consider blocking, they diagnosed the scale of k from

their model results instead of deriving the scale from the full width of the sill. As mentioned in the Introduction, the assumption of $k/m \sim \alpha$ scales the intrinsic frequency of $\omega \sim \alpha N$ (Klymak et al., 2010a). Therefore, we assume that the unsteady lee wave is phenomenologically the same as the arrested lee wave. Although a discussion of the theoretical validity of the unsteady lee wave is beyond the scope of this paper, the intrinsic frequency of $-kU_0$, instead of $-kU_0 \pm \sigma_f$ derived by Tanaka et al. (2010), is consistent with the theory of the arrested lee wave under the assumption $k/m \sim \alpha$.

The LAIWs observed and numerically reproduced in the present study also have features in common with arrested lee waves. The negative density anomalies caused by the LAIWs have a similar aspect ratio to the top of the sill topography, and the estimated intrinsic frequency is higher than the tidal frequency, consistent with the conditions permitting lee waves to develop. Although we assume that the arrested and unsteady lee waves are phenomenologically the same, the characteristics of the LAIW in the Urup Strait are more readily explained in terms of the theory of arrested lee waves than that of unsteady lee waves.

However, there is a difference in topographic parameter range between the Urup Strait and the analyses by Klymak et al. (2010a). The water depth at the sill-top is shallower (~100 m) than the vertical scale of the wavelength of the lee wave ($2\pi U_m/N \sim 1600$ m with $N = 8 \times 10^{-3}$ s^{-1} and $U_m = 2$ m s^{-1}) assumed in Klymak et al. (2010a). Although the vertical scale estimated from the parameters at the sill-break ($2\pi U/N \sim 880$ m with $N = 4.8 \times 10^{-3}$ s^{-1} and $U = 0.67$ m s^{-1}) is comparable with that of the LAIWs (twice the vertical scale of the negative potential density anomaly of 400–500 m; Fig. 2, Fig. 5 and Fig. 10), it is obvious that the observed and modeled LAIWs are not the high-mode waves examined by Klymak et al. (2010a).

Another question is how the amplitude of the arrested waves in the Urup Strait becomes so large. Although the strong tide–topography interaction is fundamentally responsible, we suggest that two underlying processes catalyze the amplification. The first is the intensification of TTWs. The energy of the barotropic tide with diurnal frequency is primarily fed into the TTWs, and stays on the topography. The clockwise rotation of the flow observed and modeled at Station UC in the Urup Strait is consistent with the occurrence of the TTWs. The sheared flow of the TTWs effectively interacts with the tall sill of the Urup Strait that is likely to block the barotropic tide. The critical role of TTWs in driving the high energy dissipation rates in the Kuril Straits was also indicated by Tanaka et al. (2010) through the experimental result that the energy dissipation is halved when $f = 0$. We assume that this is because the energy conversion from barotropic tide to TTWs does not occur, which would otherwise be followed by enhancement of the cross-sill flows. However, dissipation hot spots at the same sill-flank areas with lower magnitudes that are predicted with $f = 0$ (Tanaka, 2010) suggest that direct breaking of internal waves at the lee-side of the topography is still the primary cause of energy dissipation.

Second, if the velocity of the tidal flow over the sill exceeds the phase speed of the internal waves (i.e., the internal Froude number exceeds unity), then energy accumulates on the lee-side of the sill. This mechanism was proposed by Hibiya (1986) for tidal flow over a small obstacle. Although internal waves with diurnal frequency cannot exist in the Kuril Straits, the present study has shown that the intrinsic frequency of the LAIWs in the Urup Strait can be superinertial. The occurrence of freely propagating inertia-gravity waves in the subinertial area is consistent with Katsumata and Hibiya's (2002) analytical study of the tide–topography interaction in a rotating channel. While the flow with Froude number $\geqslant 1$ traps all internal waves propagating upstream, weaker flows also arrest those with higher vertical modes that have slower phase speeds, which was the key point of the parameterization by Klymak et al. (2010b).

To examine this second hypothesis broadly in the Kuril Straits, we compare the phase speed of first-mode internal waves in the non-rotating limit as calculated by the initial model density field and the maximum magnitude of the barotropic velocity across the topography during the 10th model day (Fig. 11). Although the phase speed of the inertia-gravity wave is faster than that in the non-rotating limit, the large Froude number of O(10) within the shallow straits implies that even the inertia-gravity waves are trapped there. We assume that kinetic energy is concentrated on the lee-side of the sills by these hydraulically supercritical flows, which amplifies the waves and results in their breaking.

Vertical mixing in the Kuril Straits

While we have focused on the variability around the Urup Strait, the discussion is directly applicable to other shallow straits. In the Rashowa Strait (sill-top depth of ~500 m) in the northern part of the Kuril Straits, LAIWs were observed in the lee-side of the strait accompanying prominent patches of density overturn (Dr. Satoshi Osafune, Japan Agency for Marine-Earth Science and Technology pers. comm.), consistent with our suggestion. The model used in the present study (Tanaka et al., 2010) has predicted similar variability in potential density, horizontal velocity, and energy dissipation rates for other shallow straits, with LAIWs on the lee-side of the sills and high energy dissipation rates (not shown).

However, high energy dissipation rates are not only found in shallow straits. In Fig. 4, vertically integrated energy dissipation rates higher than 1 W m^{-2} are predicted within the Bussol' Strait ($x = 340$–420 km) and on the bank (also referred to as the Vytiaz ridge) lying on the Pacific side of the main ridge.

Direct microstructure observations at the top of the sill at the western end of the Bussol' Strait are shown by Yagi and Yasuda (2012), and observations and model data at three sill-flank points around the seamounts within the strait are investigated by Tanaka et al. (2014). In addition, Yagi et al. (2014) estimated the

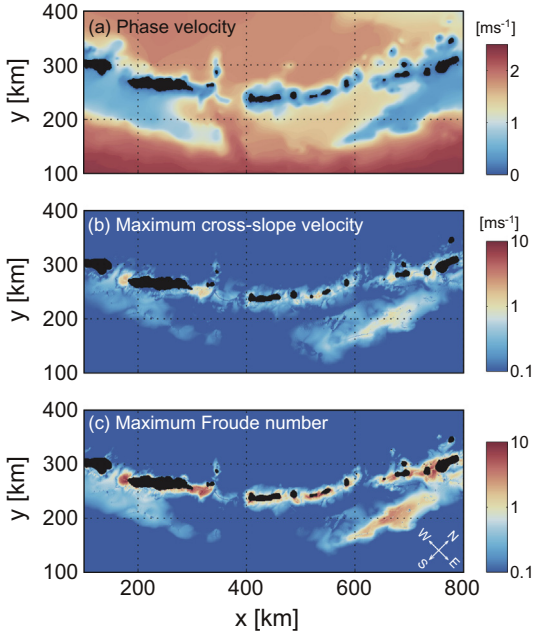

Fig. 11. Distribution of (a) phase velocity of the first-mode internal waves in the non-rotating limit, (b) maximum magnitude of barotropic velocity across the topography, and (c) maximum Froude number as calculated by dividing (b) by (a).

distribution of ε by applying a method using density inversions to tide-resolving density observations. Yagi and Yasuda (2012) and Yagi et al. (2014) found enhanced ε exceeding 10^{-6} W kg^{-1} in the 600–1300 m layer at the top of the sill. They suggested that low-mode shear of TTWs and mean flows were responsible for this enhanced mixing. Tanaka et al. (2014) similarly concluded that the low-mode shear of the TTWs causes elevated vertical mixing, although energy dissipation rates are relatively low over the northwestern and southeastern flanks of the seamount. However, although Tanaka et al. (2014) detected the propagation of the TTWs around the seamount, correlation coefficients between the vertical shear associated with the low-mode TTWs and energy dissipation rates are not high enough to enable us to explain the occurrence of strong turbulent mixing without considering additional mechanisms. We therefore presume that the interaction between the topography and a cross-topography component of TTWs is significant: sheared TTWs not only break directly as suggested by Yagi and Yasuda (2012) and Tanaka et al. (2014), but also generate internal waves even in deep waters. This presumption is consistent with the model results in that the dissipation hot spots are distributed over the sill-flanks and the areas where isobaths are inflected (Fig. 4).

The energy dissipation caused by the direct breaking of arrested lee waves considered by Klymak et al. (2010b) scales with the cube of the barotropic forcing. Assuming that this scaling represents the energy dissipation in the Kuril and Aleutian Straits where the diurnal tide is dominant, the variations in the energy dissipation caused by the 18.6-year nodal tidal cycle should be substantial: 11% and 19% of the modulation rate of the K_1 and O_1 constituents yield up to 37% and 69% variations in the energy dissipation, respectively. However, estimates of the magnitudes of the energy dissipation require the complete expression for the baroclinic energy production over steep topography. The parameterization used by Klymak et al. (2010b) that explained the energy dissipation at the Kauai ridge employed a formulation for a superinertial tide over a knife-edge topography (Llewellyn Smith and Young, 2002). However, this is not applicable to the subinertial tides of the Kuril and Aleutian Straits. Note, though, that the numerical model used by Tanaka et al. (2010) predicted that more than 80% of tidal energy was dissipated locally, a much higher value than the 30% suggested for the semidiurnal internal tides (e.g., St. Laurent et al., 2002).

The present study has shown that tidal mixing is extremely strong within the Urup Strait, and possibly in other shallow Kuril Straits. Because the strong mixing is generally concentrated within the LAIWs, the volume transport is likely to occur within a specific layer (Itoh et al., 2011). Even though the season and lunar phase are different for the observations in 2007 (Itoh et al., 2011) and 2010 (present study), the strong mixing is confined within the same layer of 26.6–26.7 σ_θ. Therefore, we confirm that the layer of intermediate waters in the Sea of Okhotsk and the North Pacific with a potential density range of 26.6–26.7 σ_θ becomes thicker in the shallow Kuril Straits including the Urup Strait. However, the thickening of intermediate waters at greater densities is likely to occur in deeper straits, because the layers of enhanced mixing were found at deeper layers in these straits (Ono et al., 2007; Yagi and Yasuda, 2012; Tanaka et al., 2013). Future studies incorporating intensive observations and higher-resolution numerical experiments resolving wave breaking processes will aim to quantify the water mass formation and its impact on ecosystems and climate.

Acknowledgements

The authors thank the captain, officers, and crew of the R/V *Professor Khromov* and all onboard scientists for their help with observations. This research was carried out under the Joint Research Program of the Pan-Okhotsk Research Center, Institute of Low Temperature Science, Hokkaido University, and supported by the Ministry of Education, Science, Sports and Culture of Japan via Grants-in-Aid for Scientific Research (KAKENHI) (S) 20221002, (B) 23310002, Innovative Areas 24121002, and (A) 25257206.

References

Garrett, C., Kunze, E., 2007. Internal tide generation in the deep ocean. Annual Review of Fluid Mechanics 39, 57–87.
Gill, A.E., 1982. Atmosphere-Ocean Dynamics. Academic Press, New York, NY, 662 pp..
Hibiya, T., 1986. Generation mechanism of internal waves by tidal flow over a sill. Journal of Geophysical Research 91, 7697–7708.
Itoh, S., Yasuda, I., Nakatsuka, T., Nishioka, J., Volkov, Y.N., 2010. Fine- and microstructure observations in the Urup Strait, Kuril Islands, during August 2006. Journal of Geophysical Research 115, C08004. http://dx.doi.org/10.1029/2009JC005629.
Itoh, S., Yasuda, I., Yagi, M., Osafune, S., Kaneko, H., Nishioka, J., Nakatsuka, T., Volkov, Y.N., 2011. Strong vertical mixing in the Urup Strait. Geophysical Research Letters 38, L16607. http://dx.doi.org/10.1029/2011GL048507.
Katsumata, K., Hibiya, T., 2002. Internal wave generation by tidal flow over a sill in a rotating channel. Journal of Geophysical Research 107, 3176. http://dx.doi.org/10.1029/2001jc001096.
Katsumata, K., Yasuda, I., Kawasaki, Y., 2001. Direct current measurements at Kruzenshterna Strait in summer. Geophysical Research Letters 28, 319–322. http://dx.doi.org/10.1029/2000GL011489.
Katsumata, K., Ohshima, K.I., Kono, T., Itoh, M., Yasuda, I., Volkov, Y.N., Wakatsuchi, M., 2004. Water exchange and tidal currents through the Bussol' Strait revealed by direct current measurements. Journal of Geophysical Research 109, 1–11.
Kitani, K., 1973. An oceanographic study of the Sea of Okhotsk, particularly in regard to cold waters. Bulletin Far Seas Fisheries Research Laboratory 9, 45–47.
Klymak, J., Legg, S., Alford, M., Buijsman, M., Pinkel, R., Nash, J., 2012. The direct breaking of internal waves at steep topography. Oceanography 25, 150–159. http://dx.doi.org/10.5670/oceanog.2012.50.
Klymak, J.M., Legg, S., Pinkel, R., 2010a. A simple parameterization of turbulent tidal mixing near supercritical topography. Journal of Physical Oceanography 40, 2059–2074. http://dx.doi.org/10.1175/2010JPO4396.1.
Klymak, J.M., Legg, S.M., Pinkel, R., 2010b. High-mode stationary waves in stratified flow over large obstacles. Journal of Fluid Mechanics 644, 321–336. http://dx.doi.org/10.1017/S0022112009992503.
Klymak, J.M., Pinkel, R., Rainville, L., 2008. Direct breaking of the internal tide near topography: Kaena ridge, Hawaii. Journal of Physical Oceanography 38, 380–399.
Legg, S., Klymak, J., 2008. Internal hydraulic jumps and overturning generated by tidal flow over a tall steep ridge. Journal of Physical Oceanography 38, 1949–1964. http://dx.doi.org/10.1175/2008JPO3777.1.
Llewellyn Smith, S.G., Young, W.R., 2002. Conversion of the Barotropic Tide. Journal of Physical Oceanography 32, 1554–1566. http://dx.doi.org/10.1175/1520-0485(2002) 032<1554:cotbt>2.0.co;2.
Mohri, K., Hibiya, T., Iwamae, N., 2010. Revisiting internal wave generation by tide-topography interaction. Journal of Geophysical Research 115. http://dx.doi.org/10.1029/2009jc005908.
Nakamura, T., Awaji, T., 2004. Tidally induced diapycnal mixing in the Kuril Straits and its role in water transformation and transport: A three-dimensional nonhydrostatic model experiment. Journal of Geophysical Research 109. http://dx.doi.org/10.1029/2003JC001850.
Nakamura, T., Awaji, T., Hatayama, T., Akitomo, K., Takizawa, T., 2000a. Tidal exchange through the Kuril Straits. Journal of Physical Oceanography 30, 1622–1644.
Nakamura, T., Awaji, T., Hatayama, T., Akitomo, K., Takizawa, T., Kono, T., Kawasaki, Y., Fukasawa, M., 2000b. The generation of large-amplitude unsteady lee waves by subinertial K-1 tidal flow: A possible vertical mixing mechanism in the Kuril Straits. Journal of Physical Oceanography 30, 1601–1621.
Nakamura, T., Isoda, Y., Mitsudera, H., Takagi, S., Nagasawa, M., 2010. Breaking of unsteady lee waves generated by diurnal tides. Geophysical Research Letters 37. http://dx.doi.org/10.1029/2009GL041456.
Ohshima, K.I., Wakatsuchi, M., Fukamachi, Y., Mizuta, G., 2002. Near-surface circulation and tidal currents of the Okhotsk Sea observed with satellite-tracked drifters. Journal of Geophysical Research 107.
Ono, K., Ohshima, K.I., Kono, T., Itoh, M., Katsumata, K., Volkov, Y.N., Wakatsuchi, M., 2007. Water mass exchange and diapycnal mixing at Bussol'Strait revealed by water mass properties. Journal of Oceanography 63, 281–291.
Osafune, S., Yasuda, I., 2006. Bidecadal variability in the intermediate waters of the northwestern subarctic Pacific and the Okhotsk Sea in relation to 18.6-year period nodal tidal cycle. Journal of Geophysical Research 111. http://dx.doi.org/10.1029/2005JC003277.
Osborn, T.R., 1980. Estimates of the local-rate of vertical diffusion from dissipation measurements. Journal of Physical Oceanography 10, 83–89.
Pinkel, R., Buijsman, M., Klymak, J.M., 2012. Breaking topographic lee waves in a tidal channel in luzon strait. Oceanography 25, 160–165.

Rabinovich, A.B., Thomson, R.E., 2001. Evidence of diurnal shelf waves in satellite-tracked drifter trajectories off the Kuril Islands. Journal of Physical Oceanography 31, 2650–2668.

St. Laurent, L.C., Simmons, H.L., Jayne, S.R., 2002. Estimating tidally driven mixing in the deep ocean. Geophysical Research Letters 29. http://dx.doi.org/10.1029/2002GL015633.

Tadokoro, K., Ono, T., Yasuda, I., Osafune, S., Shiomoto, A., Sugisaki, H., 2009. Possible mechanisms of decadal-scale variation in PO4 concentration in the western North Pacific. Geophysical Research Letters 36. http://dx.doi.org/10.1029/2009GL037327.

Talley, L.D., 1991. An Okhotsk Sea-water anomaly – implications for ventilation in the North Pacific. Deep Sea Research Part A. Oceanographic Research Papers 38, S171–S190.

Tanaka, Y., 2010. Evaluation of tidal mixing in the Kuril Straits and its impact on the formation of North Pacific Intermediate Water. PhD thesis, Dep. of Earth and Planet. Sci., Univ. of Tokyo, Tokyo.

Tanaka, Y., Hibiya, T., Niwa, Y., 2007. Estimates of tidal energy dissipation and diapycnal diffusivity in the Kuril Straits using TOPEX/POSEIDON altimeter data. Journal of Geophysical Research 112, C10021, 10010.11029/12007JC004172.

Tanaka, Y., Hibiya, T., Niwa, Y., Iwamae, N., 2010. Numerical study of K-1 internal tides in the Kuril straits. Journal of Geophysical Research 115. http://dx.doi.org/10.1029/2009JC005903.

Tanaka, Y., Yasuda, I., Osafune, S., Tanaka, T., Nishioka, J., Volkov, Y.N., 2014. Internal tides and turbulent mixing observed in the Bussol Strait. Progress in Oceanography 126, 98–108.

Thurnherr, A.M., 2011. How to process LADCP data with the LDEO software. pp. 32.

Visbeck, M., 2002. Deep velocity profiling using lowered acoustic Doppler current profilers: bottom track and inverse solutions. Journal of Atmospheric and Oceanic Technology 19, 794–807. http://dx.doi.org/10.1175/1520-0426(2002)019<0794:dvpula>2.0.co;2.

Watanabe, Y.W., Shigemitsu, M., Tadokoro, K., 2008. Evidence of a change in oceanic fixed nitrogen with decadal climate change in the North Pacific subpolar region. Geophysical Research Letters 35. http://dx.doi.org/10.1029/2007GL032188.

Yagi, M., Yasuda, I., 2012. Deep intense vertical mixing in the Bussol' Strait. Geophysical Research Letters 2011G. http://dx.doi.org/10.1029/2011GL050349. 10.1029/L050349.

Yagi, M., Yasuda, I., Tanaka, T., Tanaka, Y., Ono, K., Ohshima, K.I., Katsumata, K., 2014. Re-evaluation of turbulent mixing vertical structure in the Bussol' Strait and its impact on water masses in the Okhotsk Sea and the North Pacific. Progress in Oceanography 126, 121–134.

Yasuda, I., 1997. The origin of the North Pacific Intermediate Water. Journal of Geophysical Research 102, 893–909.